NUMERICAL PREDICTION OF THE MEAN WIND OVER WATER WAVES

Kenneth G. Dunning

NAVAL POSTGRADUATE SCHOOL
Monterey, California

THESIS

NUMERICAL PREDICTION OF THE MEAN WIND

OVER WATER WAVES

by

Kenneth G. Dunning

Thesis Advisor: R. T. Williams

March 1974

Numerical Prediction of the Mean Wind Over Water Waves

by

Kenneth G. Dunning
Lieutenant, United States Navy
B.S., Humboldt State College, 1967

Submitted in partial fulfillment of the
requirements for the degree of

MASTER OF SCIENCE IN METEOROLOGY

from the

NAVAL POSTGRADUATE SCHOOL
March 1974

ABSTRACT

Stauffer (1973) developed a theoretical model for the prediction of air flow above ocean waves. In this study his results were extended with the addition of buoyance effects and two different lower boundary conditions.

Through numerical solutions it was possible to determine that: 1) mean wind velocities at lower levels closely approximate the initial mean velocity profile for large wave numbers ($k \geq 0.45m^{-1}$) or small wave amplitudes, 2) mean wind velocities at lower levels fluctuate more from the initial mean velocity profile as the wave number decreased or the wave amplitude increases, 3) solutions were very sensitive to the level where the velocity gradient is computed in the lower boundary condition, 4) disturbance potential temperature at lower levels increases inversely with wave number, and 5) the presence of temperature fluctuations has an insignificant effect on the Reynolds stress or on the stream function. The numerical solutions show general agreement with the observational analyses of wave modified wind profiles by Davidson (1974). However, these comparisons are not conclusive because of the sensitivity in the lower boundary condition.

TABLE OF CONTENTS

LIST OF TABLES

LIST OF FIGURES

TABLE OF SYMBOLS AND ABBREVIATIONS

A - stream function amplitude (cosine coefficient)

a - wave amplitude

B - stream function amplitude (sine coefficient)

c - phase speed

c_p - specific heat at constant pressure

D - potential temperature amplitude (cosine coefficient)

E - potential temperature amplitude (sine coefficient)

G - acceleration of gravity

H - height of the boundary layer

K - coefficient of turbulent exchange of momentum which is related to the mean velocity gradient

K_θ - coefficient of turbulent exchange of heat which is related to the mean velocity gradient

k - wave number

κ - von-Karmans constant ($\kappa = 0.35$)

λ - wavelength

ν - coefficient of turbulent exchange of momentum associated with the wave-caused velocity fluctuations

ν_m - coefficient of molecular viscosity

ν_θ - coefficient of turbulent exchange of heat associated with the wave-caused velocity fluctuations

P - pressure

R_m - steady state condition

t - time

T_* - temperature scale

τ - Reynolds stress (m^2/sec^2)

θ - potential temperature fluctuation

Θ - disturbance potential temperature

Θ_o - domain mean potential temperature (Θ_o = 300°K)

U - mean horizontal velocity

u - total velocity in x-direction

u' - turbulent velocity fluctuation

U_* - dynamic velocity

W - total wind velocity

w - vertical velocity

ψ - stream function

ψ_o - stationary portion of the stream function

z - height

z_1 - false lower level

z_o - roughness parameter

ξ - vorticity ($\nabla^2\psi$)

ACKNOWLEDGEMENTS

I wish to express my deepest appreciation to Dr. R. Terry Williams for his advice and guidance during this project. Without his assistance, the research would have been much more difficult.

Gratitude is also extended to Dr. K. L. Davidson for the use of his data which was used for comparison with numerical results and his assistance as a reader in preparing for the final form of this thesis.

All numerical solutions were accomplished at the W. R. Church Computer Center, Naval Postgraduate School, Monterey, California. The advice and assistance of the computer center personnel was greatly appreciated.

I also want to thank my wife, Carol, whose support and moral encouragement made this thesis possible.

I. INTRODUCTION

The forerunner of this study (Stauffer, 1973) used a theoretical numerical model to investigate wave-related momentum transfer. The model was used to obtain the Reynolds wave stress of the perturbation-velocity field in the atmospheric layer above ocean waves. The study was similar to that of Yefimov (1970) and utilized an initial value numerical procedure similar to that of Newman (1969). Equations were solved by utilizing central differencing in general but with the turbulence terms evaluated at the previous time step. Solution separation was avoided by incorporating the Matsuno (1966) finite difference scheme every 50 time steps. Experiments were run varying the independent variables: wave number (k), dynamic velocity (U_*), roughness parameter (z_o), and the coefficient of turbulent exchange (ν). The measure of the error in the change of the stress in air (R) was computed at each time step and calculations continued until the stress reached a steady state condition defined by $R \leq 1 \times 10^{-5}$. Maximum Reynolds stress occurred at about one meter above the wave surface, and the largest momentum transfer was found to exist for the largest mean wind speeds, lowest wave numbers, and a turbulent coefficient of approximately $0.02 m^2/sec$. The magnitude of the Reynolds stress increased as the

mean wind velocity approached that of the wave phase speed in the lowest levels of the boundary layer. Thus when the wave velocity is close to the mean wind velocity in the lower levels, the disturbance energy is the greatest.

The emphasis in this study is on the changes in the mean wind which are caused by the wave stresses which were computed by Stauffer (1973). His basic model is modified to include buoyancy effects which arise during non-neutral conditions. Also the lower boundary condition was changed to include the mean wind shear. Two approximations to this boundary condition were investigated. Experiments were carried out in which the following quantities were varied: wave number (k), grid size, convergence criteria, wave amplitude (a), and lower boundary condition. It was found that the mean wind departed from the logarithmic profile in the lower region when the wave number became small and when the wave amplitude was large. Some of these variations were consistent with the observations of Davidson (1974).

II. DEVELOPMENT OF THE MODEL

Development of the model is similar to that of Stauffer (1973). The Boussinesq equations for two dimensional motion take the following form:

$$\frac{\partial \mathbb{W}}{\partial t} + \mathbb{W} \cdot \nabla \mathbb{W} = - \nabla \pi - \frac{g \Theta k}{\Theta_o} + \mathbb{F} , \tag{2.1}$$

$$\frac{\partial \Theta}{\partial t} + \mathbb{W} \cdot \nabla \Theta = - \frac{\partial}{\partial x} (\overline{u'\theta'}) - \frac{\partial}{\partial z} (\overline{w'\theta'}) , \text{ and} \tag{2.2}$$

$$\frac{\partial u}{\partial x} + \frac{\partial w}{\partial z} = 0 , \tag{2.3}$$

where

$$F_x = \frac{\partial}{\partial x} (\overline{-u'^2}) + \frac{\partial}{\partial z} (\overline{-u'w'}) ,$$

$$F_z = \frac{\partial}{\partial x} (\overline{-u'w'}) + \frac{\partial}{\partial z} (\overline{-w'^2}) ,$$

$$\pi = c_p \Theta_o (p_o/p)^K + gz ,$$

$$\Theta = T(p_o/p)^K - \Theta_o , \quad \text{and}$$

$$K = R/c_p .$$

Here $T(p_o/p)^K$ is the total potential temperature, Θ_o is the mean potential temperature for the whole region, R is the universal gas constant, c_p is the specific heat at constant pressure, x is the horizontal axis, and z is the vertical axis. Equation (2.1) is the equation of motion; equation (2.2) is the first law of thermodynamics, and equation (2.3) is the continuity equation. The

quantities u', w', and θ' are turbulent fluctuations. A straight line above a variable signifies the stationary part (time averaged) of each variable, and a wavy line represents the non-stationary part (space averaged). The velocity ($\mathbb{W}$) and the potential temperature (Θ) are broken up as follows:

$$\mathbb{W} = (U(x,t) + u(x,z,t))\,\mathbf{i} + w\,\mathbf{k} \text{ , and} \tag{2.4}$$

$$\Theta = \tilde{\Theta}(z,t) + \theta(x,z,t) \text{ .} \tag{2.5}$$

Following Yefimov (1970), the turbulent fluxes are approximated as follows:

$$-\overline{u'w'} = \tau = K\frac{\partial U}{\partial z} + \nu\left(\frac{\partial u}{\partial z} + \frac{\partial w}{\partial x}\right) \text{ ,} \tag{2.6}$$

$$\overline{u'^2} = \overline{w'^2} \text{ ,} \tag{2.7}$$

$$-\overline{w'\theta'} = K_\theta\frac{\partial \Theta}{\partial z} + \nu_\theta\frac{\partial \theta}{\partial z} \text{ , and} \tag{2.8}$$

$$-\overline{u'\theta'} = \nu_\theta\frac{\partial \theta}{\partial x} \text{ .} \tag{2.9}$$

Here K and K_θ are the coefficients of turbulent exchange for the mean fields, and ν and ν_θ are the coefficients of the wave-caused fluctuations.

The following vorticity equation is formed by taking $\mathbf{j} \cdot \nabla \times$ with equation (2.1):

$$\frac{\partial \xi}{\partial t} + U\frac{\partial \xi}{\partial x} + w\frac{\partial^2 U}{\partial z^2} + u\frac{\partial \xi}{\partial x} + w\frac{\partial \xi}{\partial z} =$$

$$\frac{\partial^2}{\partial z^2}\left[K\frac{\partial u}{\partial z} + \nu\left(\frac{\partial u}{\partial z} + \frac{\partial w}{\partial x}\right)\right] - \nu\left(\frac{\partial^3 u}{\partial x^2 \partial z} + \frac{\partial^3 w}{\partial x^3}\right) - \frac{g}{\Theta_o}\frac{\partial \theta}{\partial x} \text{ ,} \tag{2.10}$$

where

$$\xi = \frac{\partial u}{\partial z} - \frac{\partial w}{\partial x} \quad . \tag{2.11}$$

In this derivation, equations (2.3), (2.4), (2.5), (2.6), and (2.7) have been used. When equations (2.4), (2.5), (2.8), and (2.9) are introduced into equation (2.2) it becomes:

$$\frac{\partial \theta}{\partial t} + U\frac{\partial \theta}{\partial x} + w\frac{\partial \tilde{\Theta}}{\partial z} + u\frac{\partial \theta}{\partial x} + w\frac{\partial \theta}{\partial z} = \frac{\partial}{\partial z}(K_\theta \frac{\partial \tilde{\Theta}}{\partial z}) + \nu_\theta (\frac{\partial^2 \theta}{\partial x^2} + \frac{\partial^2 \theta}{\partial z^2}) . \tag{2.12}$$

These derivations have used the following assumptions:

$$\frac{\partial \tilde{\Theta}}{\partial t} \tilde{\sim} 0 \ , \quad \frac{\partial U}{\partial t} \tilde{\sim} 0 \tag{2.13}$$

Take the x-average of equations (2.10) and (2.12):

$$u\frac{\partial \xi}{\partial x} + w\frac{\partial \xi}{\partial z} = \frac{\partial^2}{\partial z^2} (K \frac{\partial U}{\partial z}) \ , \tag{2.14}$$

$$u\frac{\partial \theta}{\partial x} + w\frac{\partial \theta}{\partial z} = \frac{\partial}{\partial z} (K_\theta \frac{\partial \tilde{\theta}}{\partial z}) \ . \tag{2.15}$$

Subtract (2.14) and (2.15) from (2.10) and (2.12), respectively, and neglecting products of the fluctuation quantities gives:

$$\frac{\partial \xi}{\partial t} + U\frac{\partial \xi}{\partial x} + w\frac{\partial^2 U}{\partial z^2} = \frac{\partial^2}{\partial z^2}[\nu(\frac{\partial u}{\partial z} + \frac{\partial w}{\partial x})] - \nu[\frac{\partial^3 u}{\partial x^2 \partial z} + \frac{\partial^3 w}{\partial x^3}] - \frac{g}{\Theta_o}\frac{\partial \theta}{\partial x} \ , \tag{2.16}$$

$$\frac{\partial \theta}{\partial t} + U\frac{\partial \theta}{\partial x} + w\frac{\partial \tilde{\Theta}}{\partial z} = \nu_\theta [\frac{\partial^2 \theta}{\partial x^2} + \frac{\partial^2 \theta}{\partial z^2}] \ . \tag{2.17}$$

Since the motion is non-divergent (equation (2.3)), a stream function can be defined such that:

$$u = \frac{\partial \psi}{\partial z} , \quad w = - \frac{\partial \psi}{\partial x} . \tag{2.18}$$

When these relations are introduced into (2.16) and (2.17), they become:

$$\frac{\partial}{\partial t}[\frac{\partial^2 \psi}{\partial z^2} + \frac{\partial^2 \psi}{\partial x^2}] = -U[\frac{\partial^3 \psi}{\partial x \partial z^2} + \frac{\partial^3 \psi}{\partial x^3}] + \frac{\partial \psi}{\partial x} \frac{\partial^2 U}{\partial z^2}$$
$$+ \frac{\partial^2}{\partial z^2}[\nu(\frac{\partial^2 \psi}{\partial z^2} - \frac{\partial^2 \psi}{\partial x^2})] - \nu[\frac{\partial^4 \psi}{\partial x^2 \partial z^2} - \frac{\partial^4 \psi}{\partial x^4}] - \frac{g}{\Theta_o} \frac{\partial \theta}{\partial x} \tag{2.19}$$

$$\frac{\partial \theta}{\partial t} = -U \frac{\partial \theta}{\partial x} + \frac{\partial \psi}{\partial x} \frac{\partial \Theta}{\partial z} + \nu_\theta [\frac{\partial^2 \theta}{\partial x^2} + \frac{\partial^2 \theta}{\partial z^2}] . \tag{2.20}$$

In this study the motions are forced by a surface wave of wave number (k) and phase speed (c). Therefore, the stream function and the potential temperature departure are written as:

$$\psi = A(z,t) \cos [k(x-ct)] + B(z,t) \sin[k(x-ct)] , \tag{2.21}$$

$$\theta = D(z,t) \cos [k(x-ct)] + E(z,t) \sin[k(x-ct)] . \tag{2.22}$$

Substitute relations (2.21) and (2.22) into (2.19) and separate the cosine and sine terms. Equating the coefficients of the cosine terms gives:

$$\frac{\partial}{\partial t}[\frac{\partial^2 A}{\partial z^2} - k^2 A] = k(U-c)(Bk^2 - \frac{\partial^2 B}{\partial z^2}) + Bk \frac{\partial^2 U}{\partial z^2}$$
$$+ \frac{\partial^2}{\partial z^2}[\nu(\frac{\partial^2 A}{\partial z^2} + Ak^2)] + \nu k^2 [\frac{\partial^2 A}{\partial z^2} + Ak^2] - \frac{gkE}{\Theta_o} \tag{2.23}$$

The coefficients of the sine terms give:

$$\frac{\partial}{\partial t}[\frac{\partial^2 B}{\partial z^2} - k^2 B] = -k(U-c)(Ak^2 - \frac{\partial^2 A}{\partial z^2}) - Ak \frac{\partial^2 U}{\partial z^2}$$

$$+ \frac{\partial^2}{\partial z^2}[\nu(\frac{\partial^2 B}{\partial z^2} + Bk^2)] + \nu k^2[\frac{\partial^2 B}{\partial z^2} + Bk^2] + \frac{gkD}{\Theta_o} \qquad (2.24)$$

If the same procedure is carried out with equation (2.20), the cosine coefficients give:

$$\frac{\partial D}{\partial t} = -k(U-c)E + \frac{\partial \tilde{\Theta}}{\partial z} kB - \nu_\theta[Dk^2 - \frac{\partial^2 D}{\partial z^2}] \qquad (2.25)$$

The sine terms give:

$$\frac{\partial E}{\partial t} = -k(c-U)D + \frac{\partial \tilde{\Theta}}{\partial z} kA - \nu_\theta[Ek^2 - \frac{\partial^2 E}{\partial z^2}] \qquad (2.26)$$

Substitute (2.21) into (2.14) yields:

$$\frac{k}{2} \frac{\partial}{\partial z}[A \frac{\partial^2 B}{\partial z^2} - B \frac{\partial^2 A}{\partial z^2}] = \frac{\partial^2}{\partial z^2}(k \frac{\partial U}{\partial z}) \qquad (2.27)$$

Equation (2.15) will not be used in this study because it turns out that the temperature effects are very small. Therefore $\tilde{\Theta}$ is equal to its initial value in this study. The equations (2.23) through (2.27) form a complete set in the variables A, B, D, E, and U.

III. BOUNDARY CONDITIONS AND INITIAL CONDITIONS

Yefimov (1970) defined the boundary conditions for the lower boundary of the turbulent layer as:

$$U(\eta,t) + (x,\eta,t) = -akc \cos [k(x-ct)] , \qquad (3\text{-}1)$$

$$w(x,\eta,t) = akc \sin [k(x-ct)] , \qquad (3\text{-}2)$$

where the height of the wave surface is given by:

$$\eta = a \cos [k(x-ct)] . \qquad (3.3)$$

The deep water wave phase speed is: $c = (g/k)^{1/2}$. (3.4)

If (3.1) and (3.2) are in terms of the stream function (2.18), they can be written as:

$$U(\eta,t) + \frac{\partial \psi}{\partial z}(x,\eta,t) = akc \cos [k(x-ct)] , \qquad (3.5)$$

$$- \frac{\partial \psi}{\partial x}(x,\eta,t) = akc \sin [k(x-ct)] . \qquad (3.6)$$

The stream function and its derivatives at $z = \eta$ can be approximated by the values at $z = 0$, but $U(\eta,t)$ cannot be approximated by $U(0,t)$ since U has a very rapid change near the surface. Therefore $U(\eta,t)$ is expressed with a Taylor series expansion as:

$$U(\eta,t) = U(0,t) + \frac{\partial U}{\partial z} \eta . \qquad (3.7)$$

Substitute (2.21) into (3.5) and use (3.7) and (3.3) which gives:

$$\frac{\partial A}{\partial z}(0,t) = -a[kc + \frac{dU}{dz}] , \qquad (3.8)$$

$$\frac{\partial B}{\partial z}(0,t) = 0 \qquad (3.9)$$

The condition $U(0,t) \tilde{\sim} 0$ has been used. When (2.21) is substituted into (3.6), the following are obtained:

$$A(0,t) = ac \ , \tag{3.10}$$

$$B(0,t) = 0 \ . \tag{3.11}$$

The following boundary condition is used for the potential temperature fluctuation:

$$\theta(x,0,t) = 0 \tag{3.12}$$

This condition is not as accurate as the velocity conditions above, but the results shown later indicate that the temperature effects will be small in any case. Substituting (2.22) into (3.12) yields:

$$D(0,t) = E(0,t) = 0 \tag{3.13}$$

In order to close the problem, the following conditions are imposed at the top of the region:

$$A(H,t) = \frac{\partial A}{\partial z}(H,t) = B(H,t) = \frac{\partial B}{\partial z}(H,t) = D(H,t) = E(H,t) = 0 \ , \tag{3.14}$$

where $z = H$ is the upper boundary.

The initial conditions are given by:

$$A(z,0) = ac \sinh[k(H_1 - z)]/\sinh kH_1 \ , \tag{3.15}$$

$$B(z,0) = 0 \ , \tag{3.16}$$

$$D(z,0) = 0 \ , \tag{3.17}$$

$$E(z,0) = 0 \ , \tag{3.18}$$

and

$$U(z,0) = \frac{U_*}{\kappa} \ln\left(\frac{z}{z_o} + 1\right) \ , \tag{3.19}$$

where: $H_1 = H-\Delta z$, U_* = dynamic velocity, z_o = roughness parameter, $\kappa = 0.35$ = von-Karmen's constant, and a = wave amplitude. The equations give an irrotational initial state with no temperature fluctuations. The initial mean wind is logarithmic.

The following fields which are independent of time take the following form:

$$K = \kappa U_* z \ , \tag{3.20}$$

$$\tilde{\Theta} = \frac{T_*}{\kappa} \ln \left(\frac{z}{z_o} + 1\right) \ , \tag{3.21}$$

where T_* is the temperature scale.

IV. NUMERICAL PROCEDURES

Centered finite differences are introduced into equations (2.23) through (2.26) with the exception that the turbulence terms are evaluated at the previous time step. The left hand side of the equations are solved for the time tendencies with the Guass elimination technique which is described in Richtmyer (1957). Centered time differencing is used except that the solution is restarted every 50 time steps with the finite difference scheme developed by Matsuno (1966). This procedure eliminates solution separation.

Note that the value of U given in equation (3.19) with the coefficient given by (3.20) leads to a zero value for the right hand side of (2.27). Therefore U can be expressed as follows:

$$U(z,t) = \frac{U_*}{K} \ln\left(\frac{z}{z_o} + 1\right) + \tilde{u}(z,t) \quad . \tag{4.1}$$

Substitute (4.1) into (2.27) and integrate three times with respect to z which yields:

$$u = -\frac{1}{\nu} \int_o^z \tau \, dz \quad , \tag{4.2}$$

where $$\tau = -uw = -\frac{1}{2}k\left(\frac{\partial B}{\partial z}A - \frac{\partial A}{\partial z}B\right) \tag{4.3}$$

is the Reynolds wave stress. In this derivation the right hand side of (2.27) was rewritten and the coefficient K was replaced by the constant ν .

The boundary conditions (3.8), (3.9), (3.13), and (3.14) are applied in a straightforward manner with a one-sided derivative when required.

The time integration of the system of equations is accomplished by first solving the finite difference form of (2.23) through (2.26), and then computing the new U from equation (4.1). Integration is continued until a steady state is reached. The following quantity is used as a measure of the steadiness of the solution:

$$R = \left[\sum_{i=1}^{i-\frac{H_1}{\Delta z}} [\tau(z_i,t) - \tau(z_i,t-\Delta t)]^2 \right]^{\frac{1}{2}} \qquad (4.4)$$

The integration is continued until $R_m \geq R$, where R_m will take on three different values.

V. NUMERICAL SOLUTIONS

The following constants were used in all numerical integrations:

$$\begin{aligned} U_* &= 0.167 \text{ m sec}^{-1} , \\ z_o &= 7.9 \times 10^{-5} \text{ m} , \\ \nu &= 0.24 \text{ m}^2 \text{ sec}^{-1} . \end{aligned} \tag{5.1}$$

Three forms of the boundary condition (3.8) were used in these numerical integrations. Stauffer (1973) used the following condition which neglects the $\frac{\partial U}{\partial z}$ term:

$$\frac{\partial A}{\partial z}(0,t) = -akc \text{ .} \tag{5.2}$$

The direct use of (3.19) in equation (3.8) leads to a singularity when applied at $z = 0$. In a private communication, Professor R. Davis has suggested that this problem can be alleviated by computing the derivative at a false level $z = z_1$. In this case the boundary condition becomes:

$$\frac{\partial A}{\partial z}(0,t) = -a\left[kc + \frac{U_*}{\kappa(z_1 + z_o)}\right] . \tag{5.3}$$

This formula reduces to (5.2) when z_1 is very large. This procedure does not take into account changes in the mean wind near the surface through $\tilde{u}$.

A third boundary condition was used which changes as the mean wind changes. This takes the form:

$$\frac{\partial A}{\partial z}(0,t) = -a[kc + \frac{U(\Delta z,t) - U(0,t)}{\Delta z}] \quad (5.4)$$

Numerical solutions were obtained varying six independent parameters as shown in Table I. These were wave number (k), wave amplitude (a), measure of the error in the change of the stress in air (R_m), false level (z_1), temperature scale (T_*), and the boundary condition $\frac{\partial A}{\partial z}(0,t)$. Experiments were carried out as exhibited in Table II for the different values shown in Table I.

Figures 1 and 2 show the distribution of mean wind velocity (U) with height (z) for series 1 and 2, respectively. These experiments use the lower boundary condition used by Stauffer (1973). Both figures show that the mean wind is close to the logarithmic profile for the largest wave numbers. They also show large variations as the wave number decreases. These departures are principally in the lower layers below approximately six meters. The smallest wave number ($k = 0.050\ m^{-1}$) shows a much larger velocity than the logarithmic profile with a first maximum at approximately 1.5 meters. The character of the solutions for the two values of R_m are similar, but for particular wave numbers there are considerable differences.

Figures 3 and 4 represent series 3 for wave numbers $k = 0.35\ m^{-1}$ and $k = 0.20\ m^{-1}$, respectively. These actually represent the Reynolds wave stress (τ) as a function of height. Curve six in each figure is for the case z_1 = infinity which corresponds to the boundary condition used

TABLE I. Values of the variables considered in the numerical experiments.

$k\ (m^{-1})$	$a\ (m)$	$z_1\ (m)$	R_m	$\frac{\partial A}{\partial z}(0,t)$	T_*
0.050	0.10	0.025	10^{-5}	$-akc$	0.00
0.075					
0.100	0.25	0.075	10^{-6}	$-a\left(kc + \frac{U_*}{\kappa(z_1 + z_o)}\right)$	0.15
0.125					
0.150	0.50	0.225	10^{-7}		
0.175				$-a\left(kc + \frac{U(\Delta z,t)-U(0,t)}{\Delta z}\right)$	-0.15
0.200	0.67	0.675			
0.225					
0.250	1.00	2.025			
0.275					
0.300	2.00	Infinity			
0.325					
0.350					
0.375					
0.400					
0.42535					
0.450					
0.475					
0.500					
1.000					

TABLE II. Experimental tests that were carried out using the values in Table I.

Series No.	Variable	R_m	$\frac{\partial A}{\partial z}(0,t)$	T_*	Δz (m)	Δt (sec)
1	Wave number (k)	10^{-5}	$-akc$	0.00	0.25	0.125
2	Wave number (k)	10^{-6}	$-akc$	0.00	0.25	0.125
* 3	False level (z_1)	10^{-5}	$-a\left(kc + \frac{U_*}{\kappa(z_1+z_o)}\right)$	0.00	0.25	0.125
4	Wave number (k)	10^{-5}	$-a\left(kc + \frac{U(\Delta z,t)-U(0,t)}{\Delta z}\right)$	0.00	0.25	0.125
5	Wave number (k)	10^{-6}	$-a\left(kc + \frac{U(\Delta z,t)-U(0,t)}{\Delta z}\right)$	0.00	0.25	0.125
6	Wave number (k)	10^{-7}	$-a\left(kc + \frac{U(\Delta z,t)-U(0,t)}{\Delta z}\right)$	0.00	0.25	0.125
7	Wave number (k)	10^{-5}	$-a\left(kc + \frac{U(\Delta z,t)-U(0,t)}{\Delta z}\right)$	0.00	0.125	0.003125
** 8	Wave amplitude(a)	10^{-5}	$-a\left(kc + \frac{U(\Delta z,t)=U(0,t)}{\Delta z}\right)$	0.00	0.25	0.125
9	Wave number (k)	10^{-5}	$-a\left(kc + \frac{U(\Delta z,t)-U(0,t)}{\Delta z}\right)$	0.15	0.25	0.125

* carried out with wave number (k) = 0.350 m^{-1} and 0.200 m^{-1}

** carried out with wave number (k) = 0.400 m^{-1} and 0.150 m^{-1}

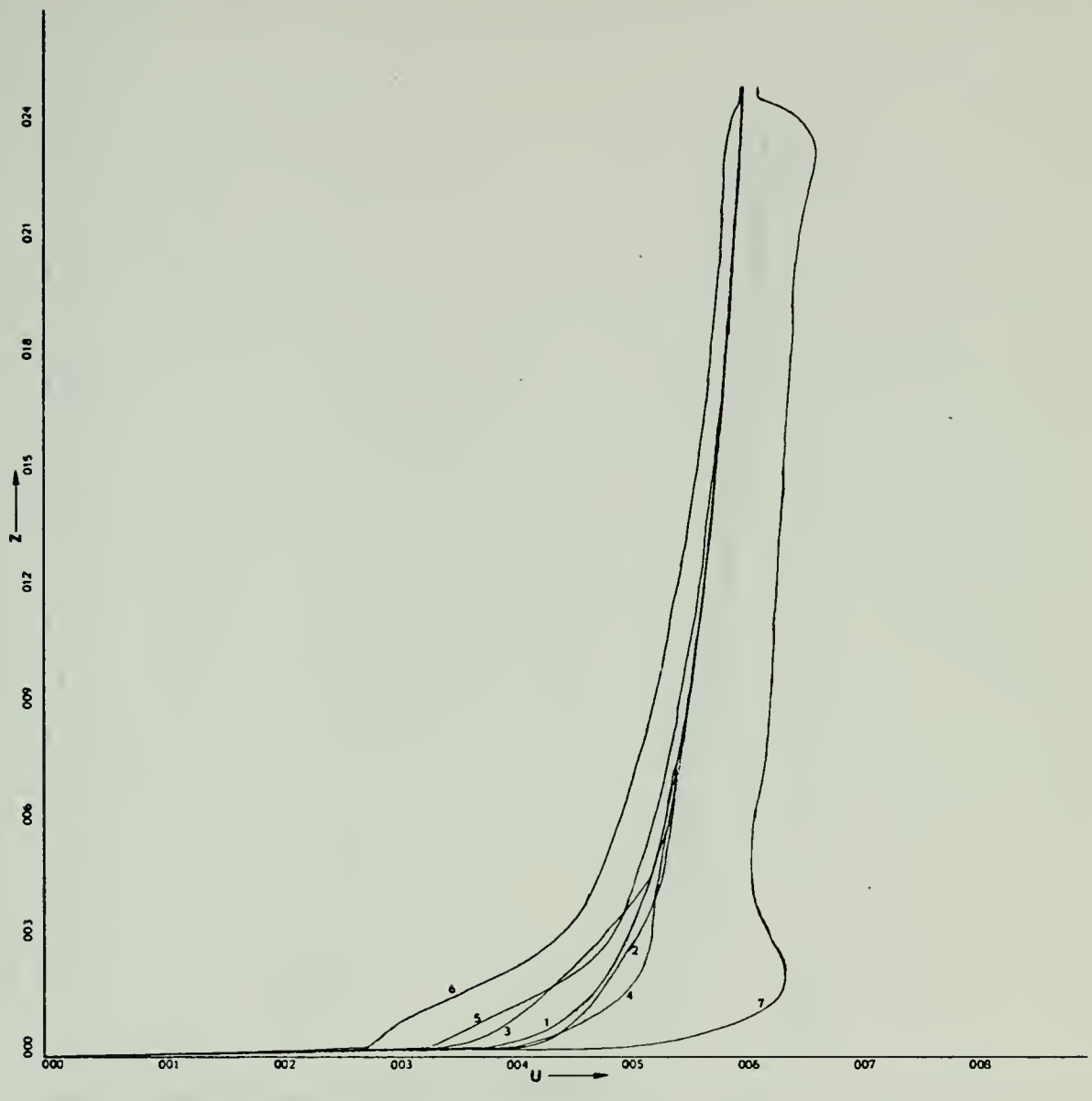

Figure 1. Distribution of the mean wind velocity (U in m sec^{-1}) with height (z in meters) utilizing series 1 for wave number (k) equal, respectively to: 1) initial mean velocity profile; 2) 0.475 m^{-1}; 3) 0.375 m^{-1}; 4) 0.275 m^{-1}; 5) 0.175 m^{-1}; 6) 0.100 m^{-1}; 7) 0.050 m^{-1}.

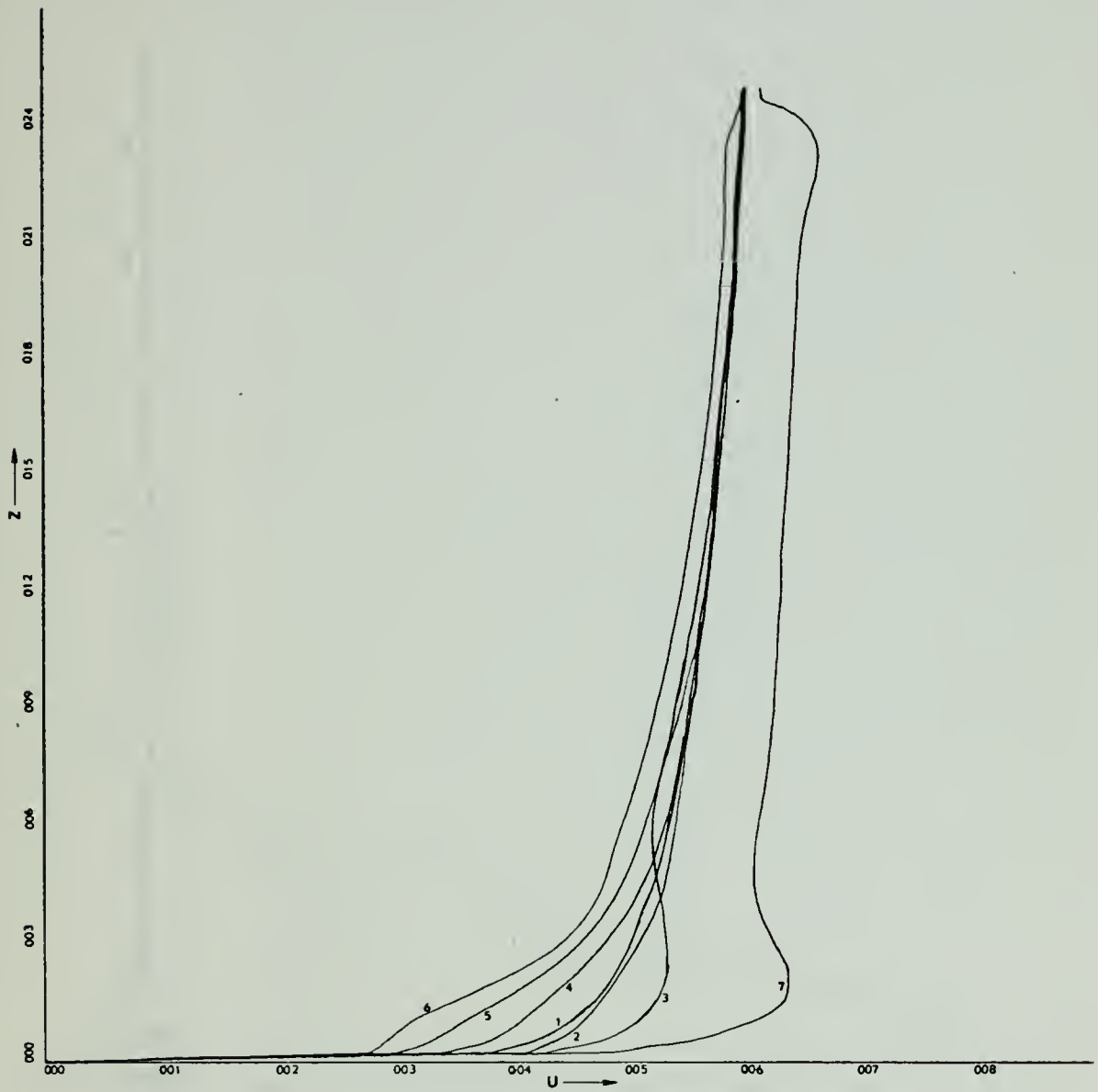

Figure 2. Distribution of mean wind velocity (U in m sec^{-1}) with height (z in meters) utilizing series 2 for wave number (k) equal, respectively, to: 1) initial mean velocity profile; 2) 0.475 m^{-1}; 3) 0.375 m^{-1}; 4) 0.275 m^{-1}; 5) 0.175m^{-1}; 6) 0.100 m^{-1}; 7) 0.050 m^{-1}.

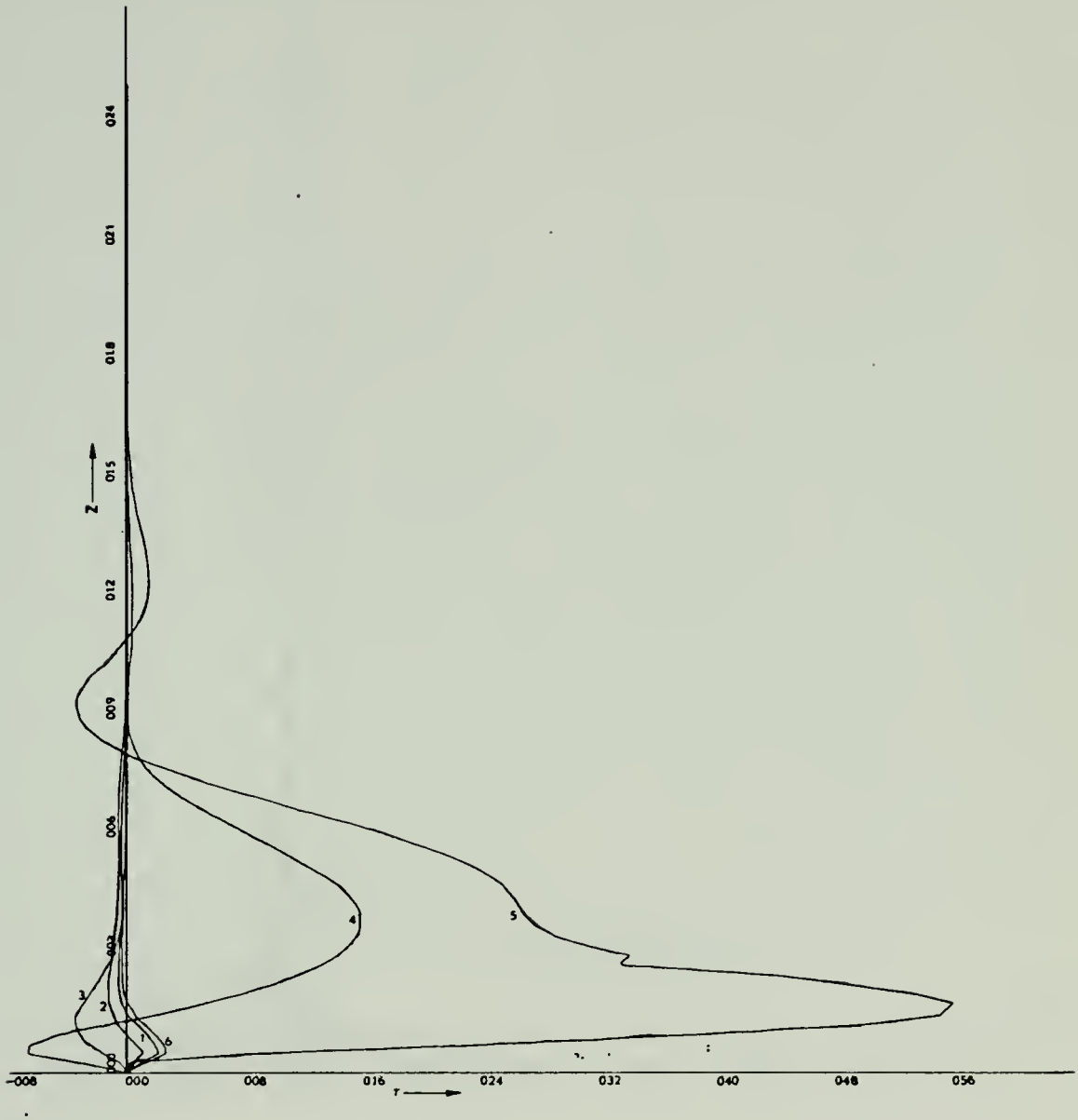

Figure 3. Distribution of the wave-caused stress (τ in 0.08 $m^2 sec^{-2}$) with height for wave number (k) equal to 0.350 m^{-1}, and utilizing series 3. Variation in z_1 is equal, respectively, to: 1) 2.025 m; 2) 0.675 m; 3) 0.225 m; 4) 0.075 m; 5) 0.025 m; 6) infinity.

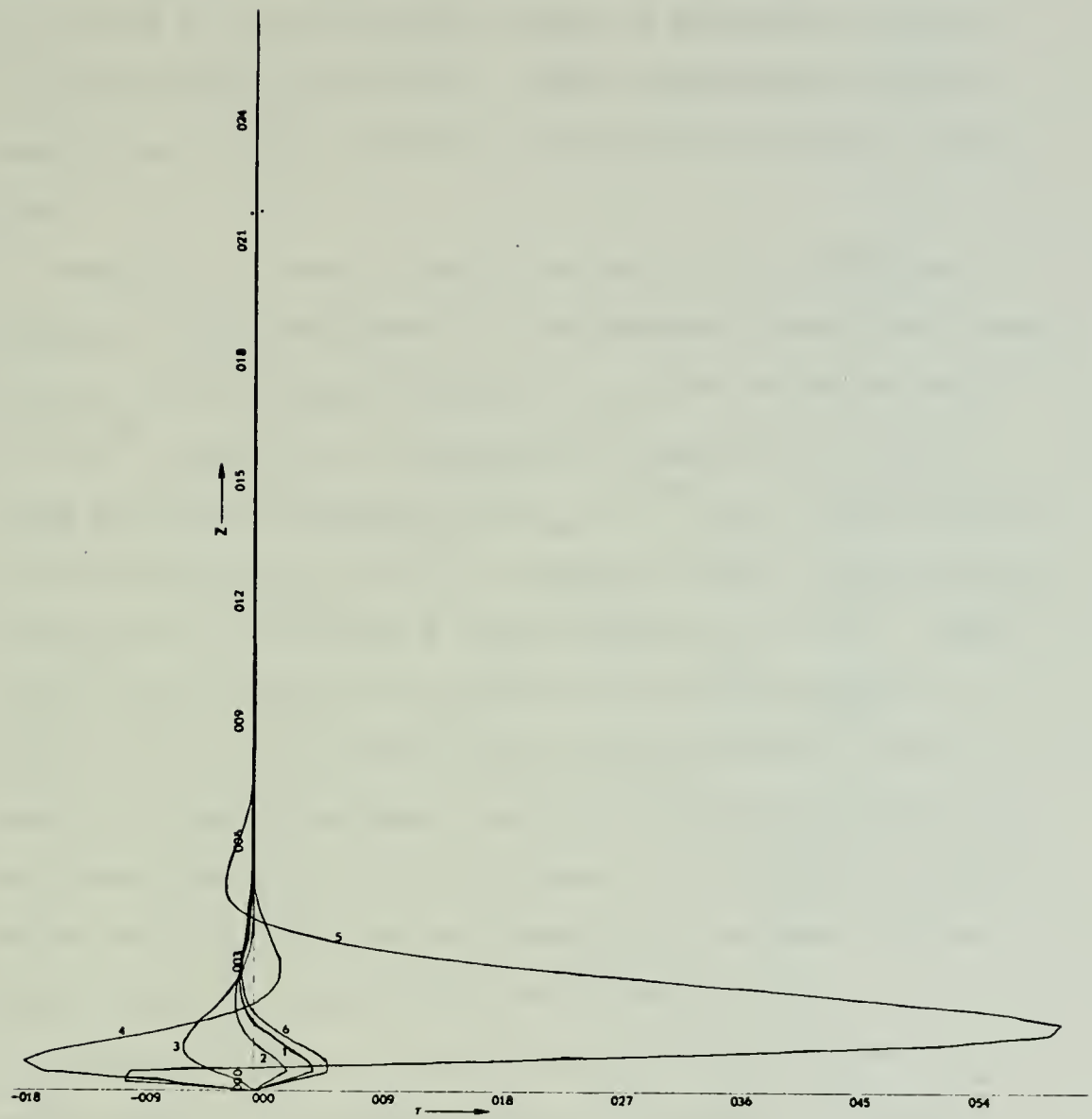

Figure 4. Distribution of the wave-caused stress (τ in 0.09 $m^2 sec^{-2}$) with height for wave number (k) equal to 0.200 m^{-1}, and utilizing series 3. Variation in z_1 is equal, respectively to: 1) 2.025 m; 2) 0.675 m; 3) 0.225m; 4) 0.075 m; 5) 0.025 m; 6) infinity.

by Stauffer (1973). These two curves are very similar to the curves for z_1 = 2.025 m. As z_1 decreases, the curve changes rapidly in such a way that the maximum stress for z_1 = 0.025 m is at least one order of magnitude greater than the case z_1 = infinity. These experiments show the sensitivity of the solutions to this lower boundary condition.

Series 4, 5, and 6, which use the finite difference estimate of the wind shear in the boundary condition, were carried out with three values of R_m. The solutions for $R_m = 10^{-5}$ and $R_m = 10^{-6}$ showed some significant differences while the solutions for $R_m = 10^{-7}$ were nearly identical for those of $R_m = 10^{-6}$. Figures 5 and 6 show the mean wind profile for series 5 which employs $R_m = 10^{-6}$. These figures show that for $k \geq 0.450\ m^{-1}$ the wind profile is very close to the initial mean velocity profile. Also note the large departures from the logarithmic profile at low levels for $k = 0.1\ m^{-1}$ or less. A disturbing feature of the solutions is the oscillation of the mean wind between adjacent values of the wave numbers.

Figure 7 shows the solutions for the mean wind for series seven. These solutions are the same as those of series 4 except that the grid size has been cut in half and the time step has been reduced to one-fourth. These solutions are generally similar to those in figures 5 and 6, except that in the lower levels the wind is larger than the logarithmic value for $k \leq 0.42535\ m^{-1}$. These results

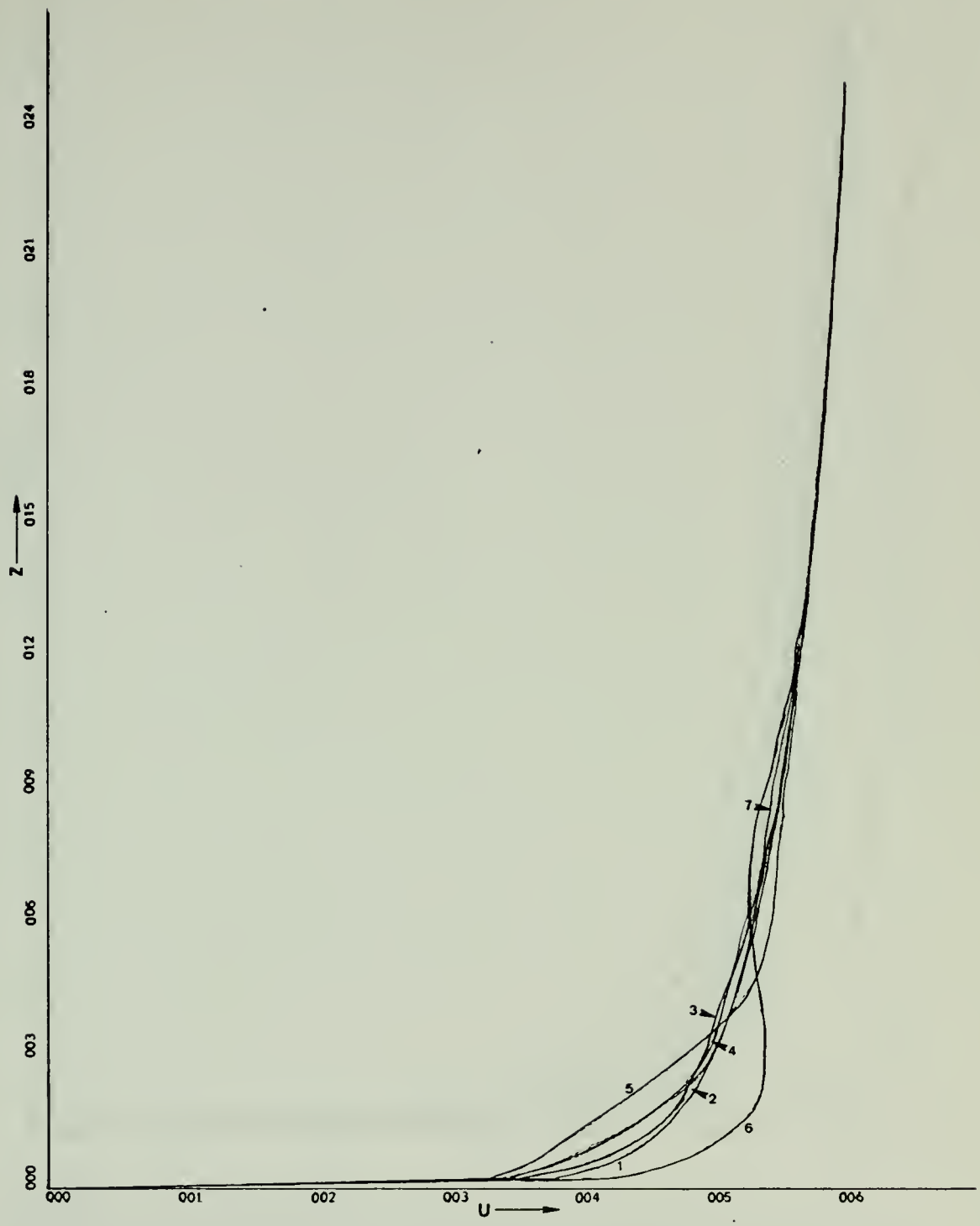

Figure 5. Distribution of the mean wind velocity (U in m sec^{-1}) with height (z in meters) utilizing series 5 fcr wave number (k) equal, respectively, to: 1) initial mean velocity profile; 2) 1.000 m^{-1}; 3) 0.500 m^{-1}; 4) 0.450 m^{-1}; 5) 0.400 m^{-1}; 6) 0.350 m^{-1}; 7) 0.300 m^{-1}.

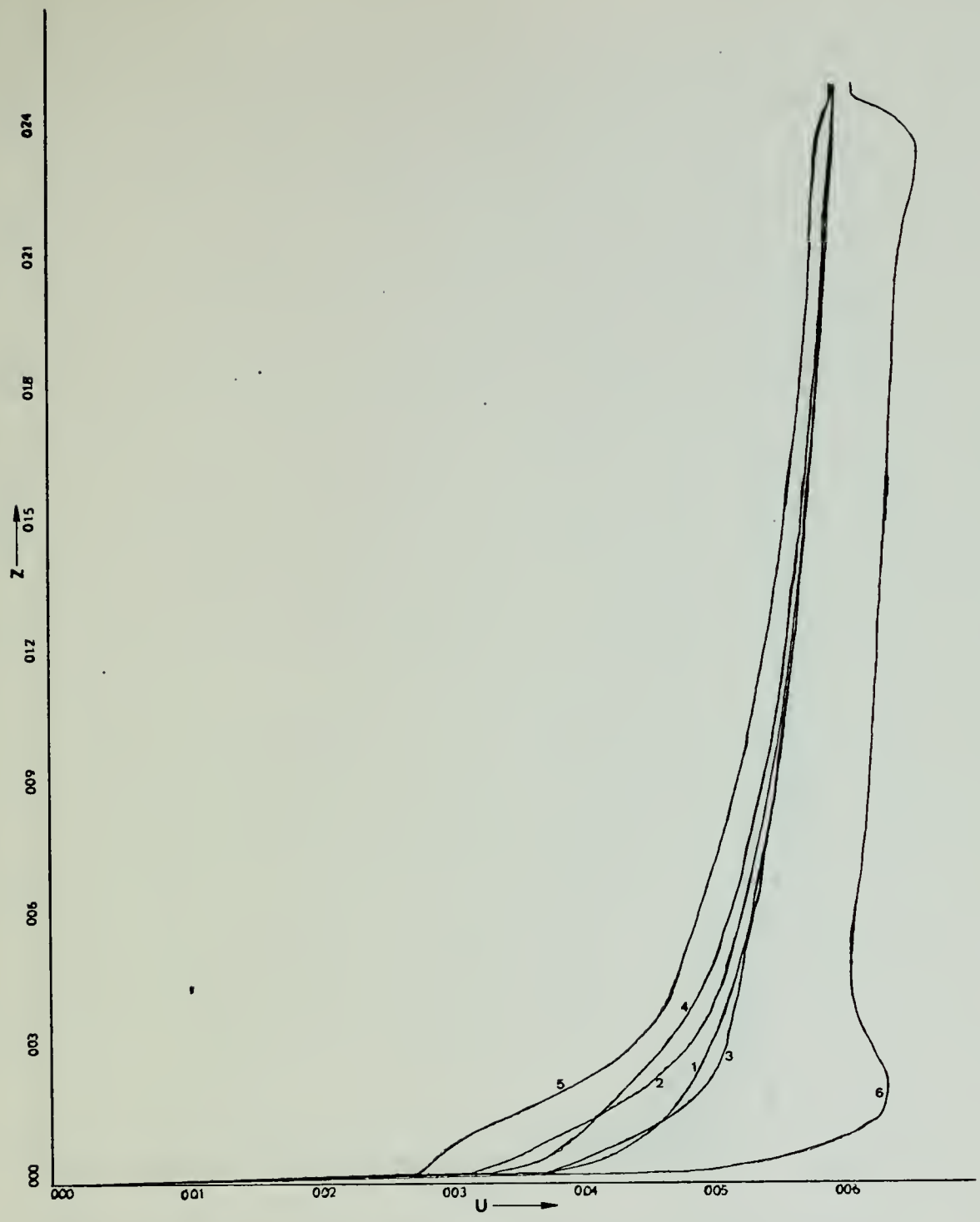

Figure 6. Distribution of the mean wind velocity (U in m sec^{-1}) with height (z in meters) utilizing series 5 for wave number (k) equal, respectively, to: 1) initial mean velocity profile; 2) 0.250 m^{-1}; 3) 0.200 m^{-1}; 4) 0.150 m^{-1}; 5) 0.100 m^{-1}; 6) 0.050 m^{-1}.

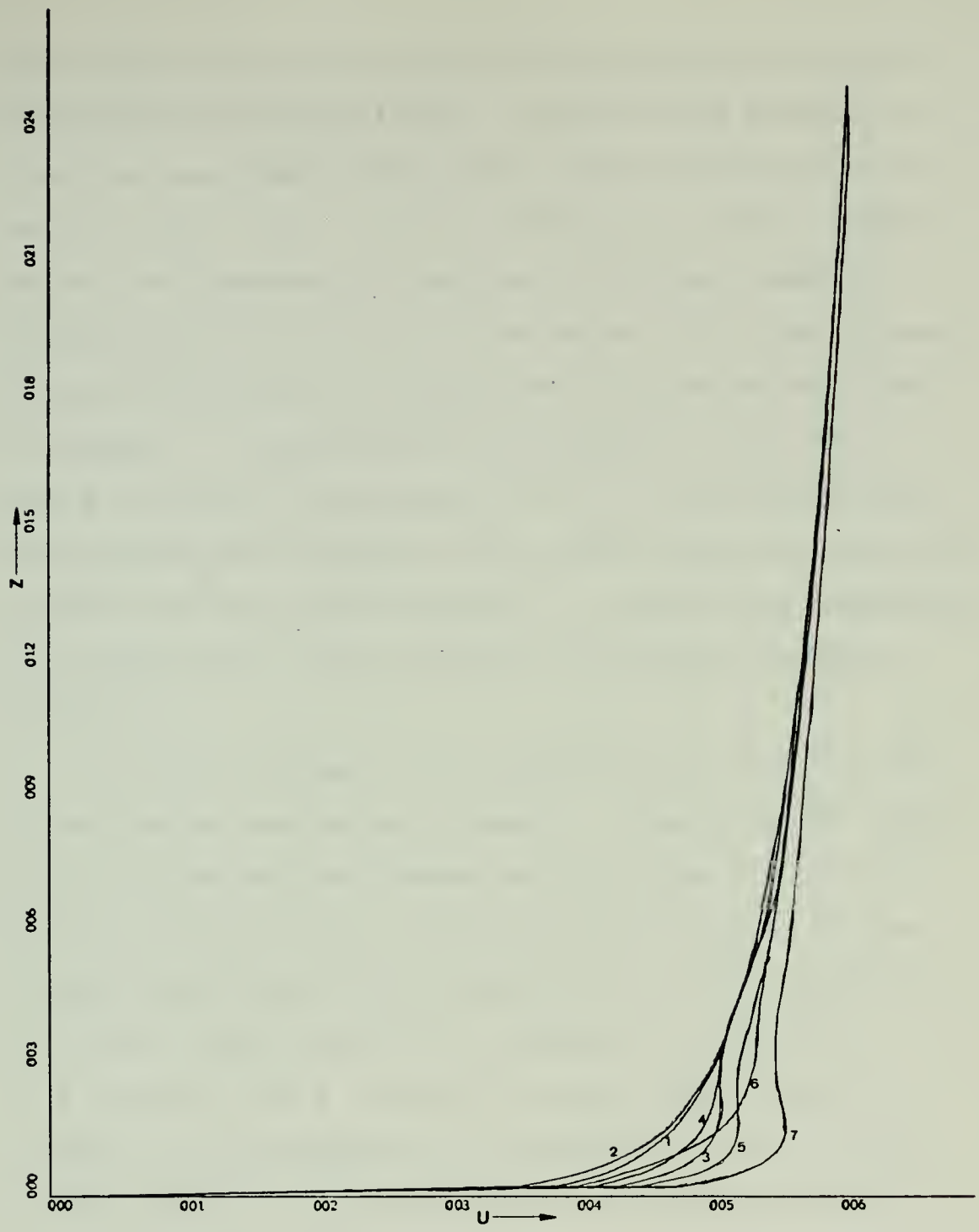

Figure 7. Distribution of the mean wind velocity (U in m sec^{-1}) with height (z in meters) utilizing series 7 for wave number (k) equal, respectively, to: 1) initial mean velocity profile; 2) 1.000 m^{-1}; 3) 0.42535 m^{-1}; 4) 0.400 m^{-1}; 5) 0.200 m^{-1}; 6) 0.175 m^{-1}; 7) 0.150 m^{-1}.

are qualitatively consistent with the empirical relation developed by Davidson (1974). His data show departures from the logarithmic wind profile which are proportional to $0.16 \left(\frac{c}{U_*} - 26.3\right)$. For this condition in these experiments, this quantity is positive for all wave numbers shown except for $k = 1.0\ m^{-1}$ for which it is slightly negative. This behavior is consistent with the curves given in figure 7. One further test was made in this series for $k = 0.200\ m^{-1}$ but with $R_m = 10^{-6}$. In that experiment the maximum wind velocity in the lower levels was very much larger than any shown in figure 7. This further emphasizes the sensitivity of the solutions to the lower boundary condition.

Figures 8 through 11 are comparisons of data already presented for certain wave numbers. Figure 8 shows identical solutions for the reduced grid size for $k = 1.0\ m^{-1}$. These solutions have a slightly smaller velocity in the lower layers than for the logarithmic profile. Figures 9, 10, and 11 which are for wave numbers $k = 0.40\ m^{-1}$, $k = 0.20\ m^{-1}$, and $k = 0.15\ m^{-1}$, respectively, show irregular variations about the logarithmic profile for different values of R_m, but systematically higher values of wind speed for $\Delta z = 0.125$ m.

Figures 12 and 13 contain the solutions from series 8 for wave numbers $k = 0.40\ m^{-1}$ and $k = 0.15\ m^{-1}$, respectively. In all other experiments the wave amplitude is given by:

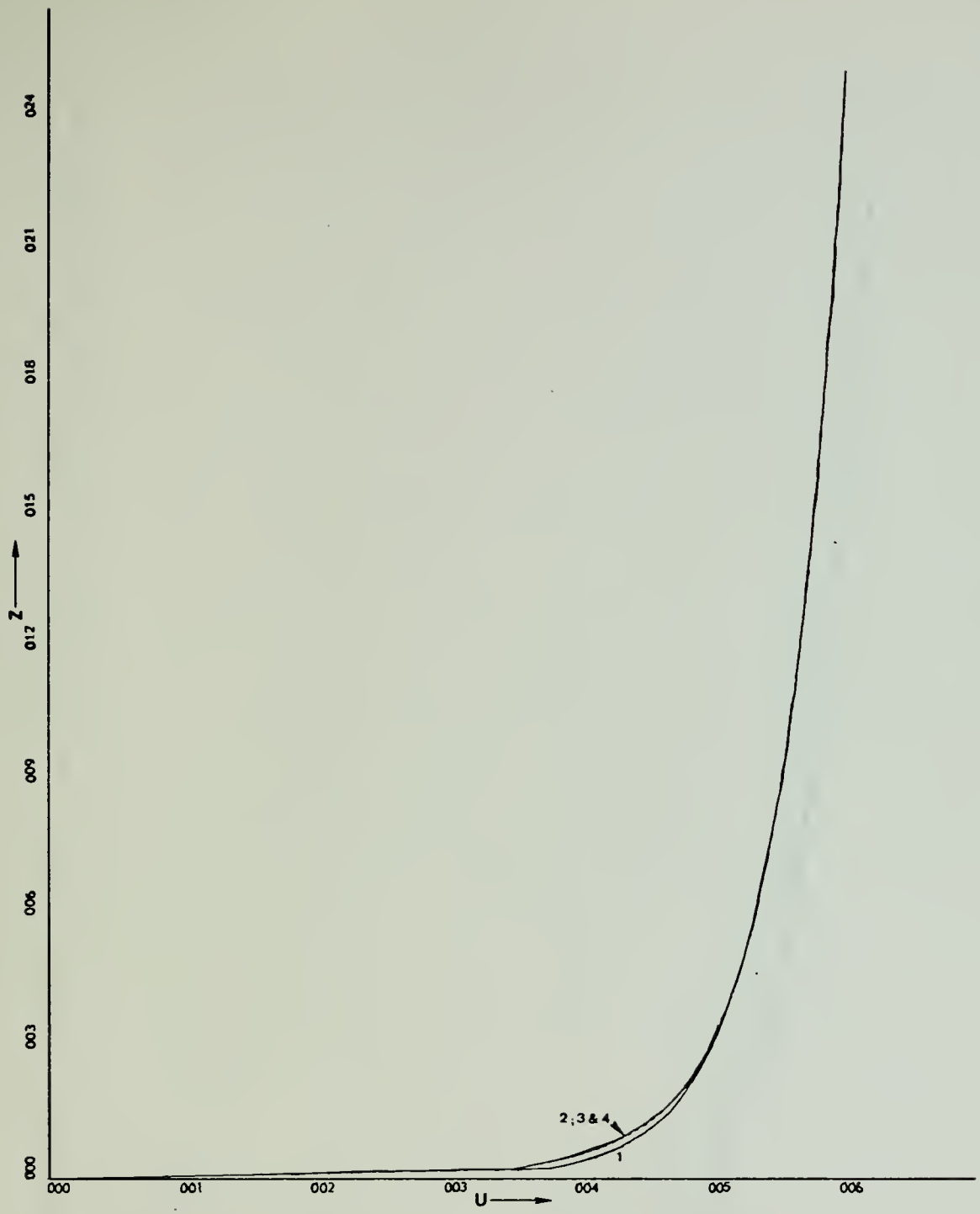

Figure 8. Distribution of the mean wind velocity (U in m sec^{-1}) with height (z in meters) for wave number (k) equal to 1.000 m^{-1}. Comparison is made where: 1) initial mean velocity profile; 2) series 4; 3) series 5 and 6; 4) series 7.

Figure 9. Distribution of the mean wind velocity (U in m sec^{-1}) with height (z in meters) for wave number (k) equal to 0.0400 m^{-1}. Comparison is made where: 1) initial mean velocity profile; 2) series 4; 3) series 5 and 6; 4) series 7.

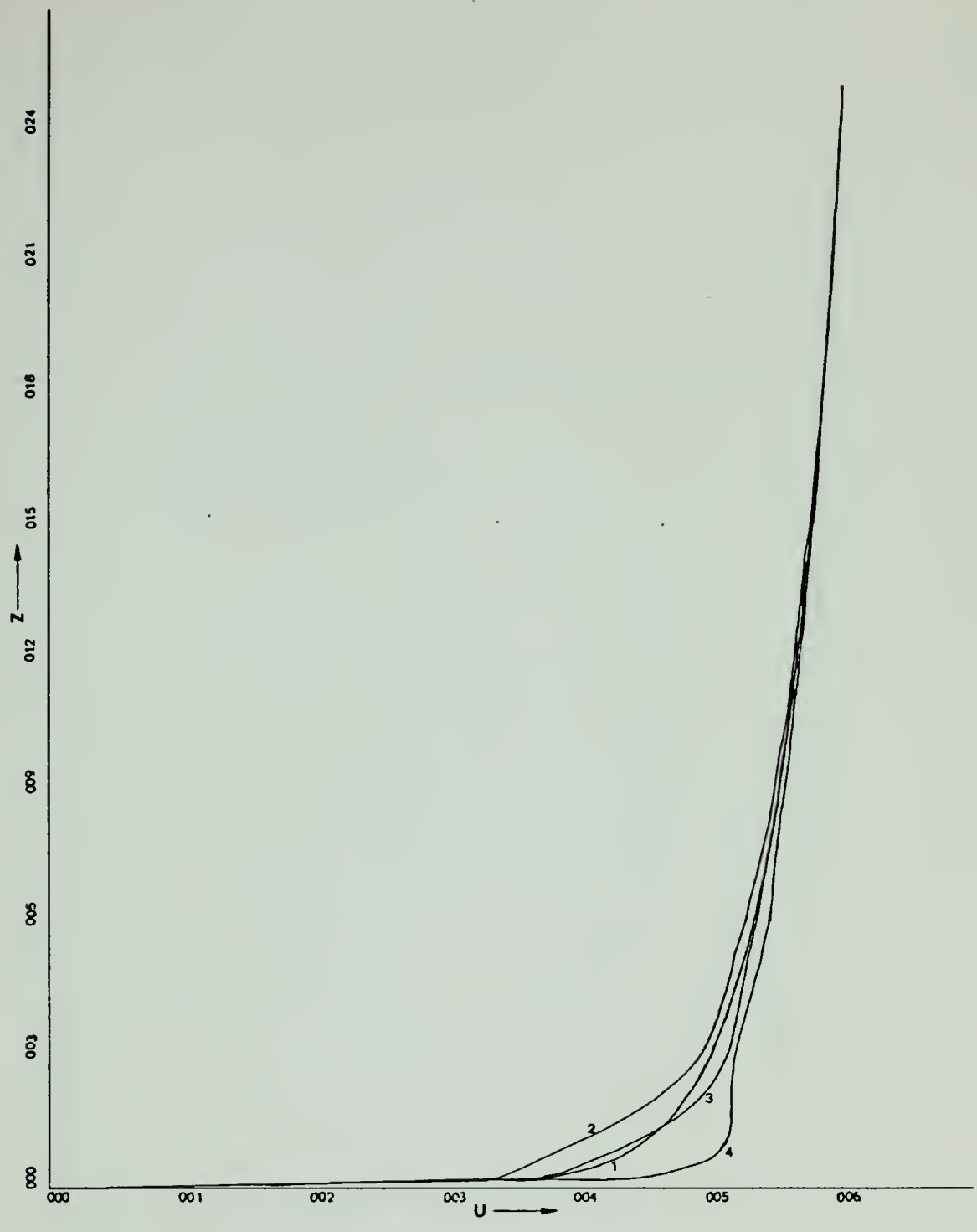

Figure 10. Distribution of the mean wind velocity (U in m sec^{-1}) with height (z in meters) for wave number (k) equal to 0.200 m^{-1}. Comparison is made where: 1) initial mean velocity profile; 2) series 4; 3) series 5 and 6; 4) series 7.

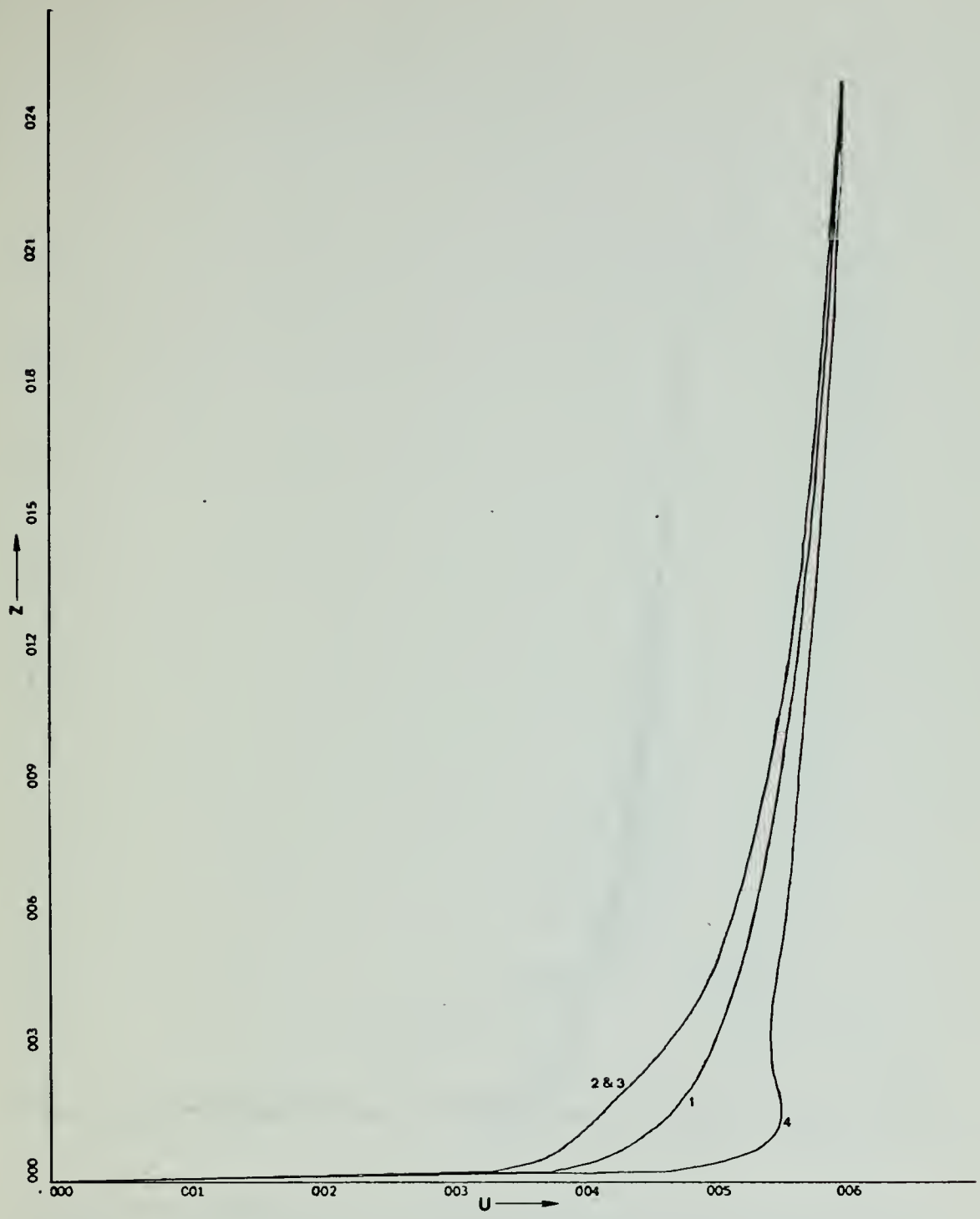

Figure 11. Distribution of mean wind velocity (U in m sec^{-1}) with height (z in meters) for wave number (k) equal to 0.150 m^{-1}. Comparison is made where: 1) initial mean velocity profile; 2) series 4; 3) series 5 and 6; 4) series 7.

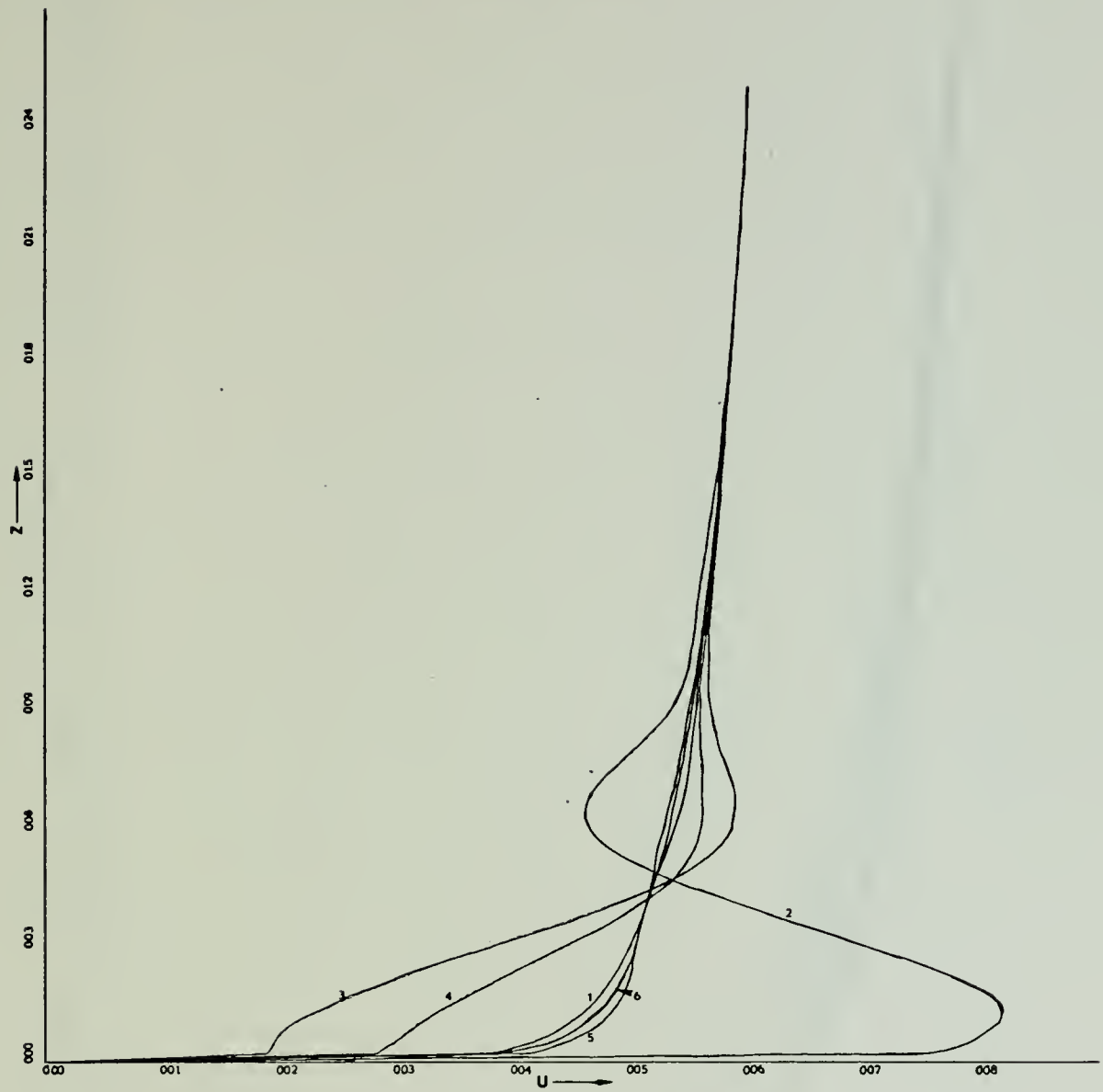

Figure 12. Distribution of the mean wind velocity (U in m sec^{-1}) with height (z in meters) utilizing series 8 for wave number (k) equal to 0.400 m^{-1}. Variation in wave amplitude (a in meters) is equal, respectively, to: 1) initial mean velocity profile; 2) 2.00 m; 3) 1.00 m; 4) 0.50 m; 5) 0.25 m= .1/k; 6) 0.10m.

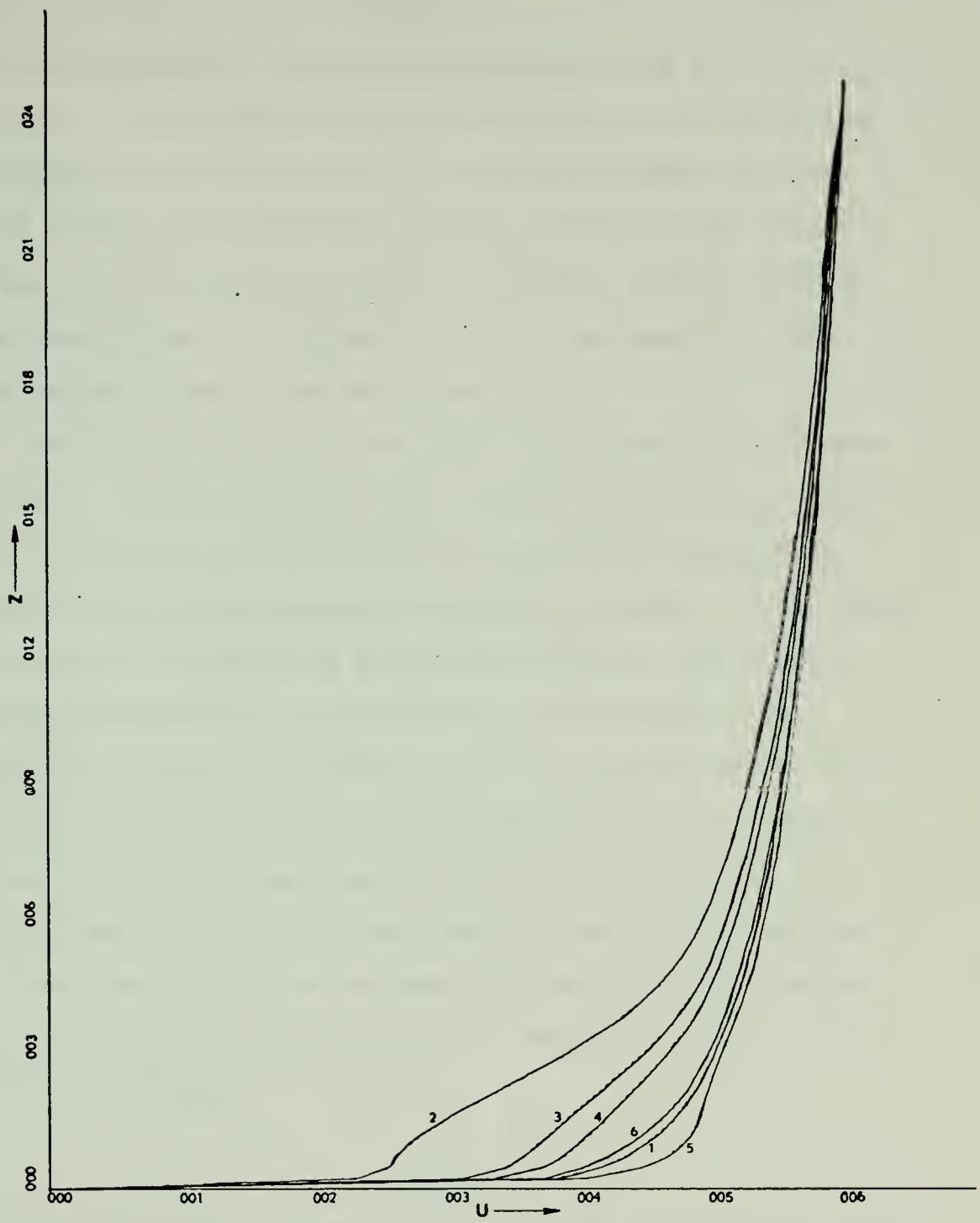

Figure 13. Distribution of mean wind velocity (U in m sec^{-1}) with height (z in meters) utilizing series 8 for wave number (k) equal to 0.150 m^{-1}. Variation in wave amplitude (a in meters) is equal, respectively, to: 1) initial mean velocity profile; 2) 2.00 m; 3) 1.00 m; 4) 0.67 m = .1/k; 5) 0.50 m; 6) 0.10 m.

$$a = 0.1\ k^{-1} \qquad (5.5)$$

In these figures, the amplitude ranges from 0.10 m to 2.00 m. The smaller values of amplitude gives wind profiles which are very close to the logarithmic profile. The larger wave amplitudes lead to increasingly larger departures from the logarithmic profile. This is to be expected since $\tilde{u}$ is proportional to the square of the disturbance amplitude (equation 4.2).

Figure 14 contains the disturbance potential temperature as a function of z, from series 9 with three values of k. These curves show that the largest temperature amplitudes occur at about one meter in height; above these maxima the temperature decreases rapidly. The largest amplitude occurs for the smallest wave number. The numerical solutions showed that the stream function amplitudes were not significantly affected by the presence of temperature fluctuations. This was true for both $T_* = +0.15$ and $T_* = -0.15$. This behavior may be interpreted as follows. If it is assumed that the horizontal advection is balanced by the vertical advection, then equation (2.17) becomes:

$$\theta = \frac{1}{U-c} \frac{\partial \tilde{\Theta}}{\partial z} \psi \ . \qquad (5.6)$$

This expression is used to estimate the last term in (2.19). It can be seen that the buoyance term will be much smaller than the vorticity advection term with the possible

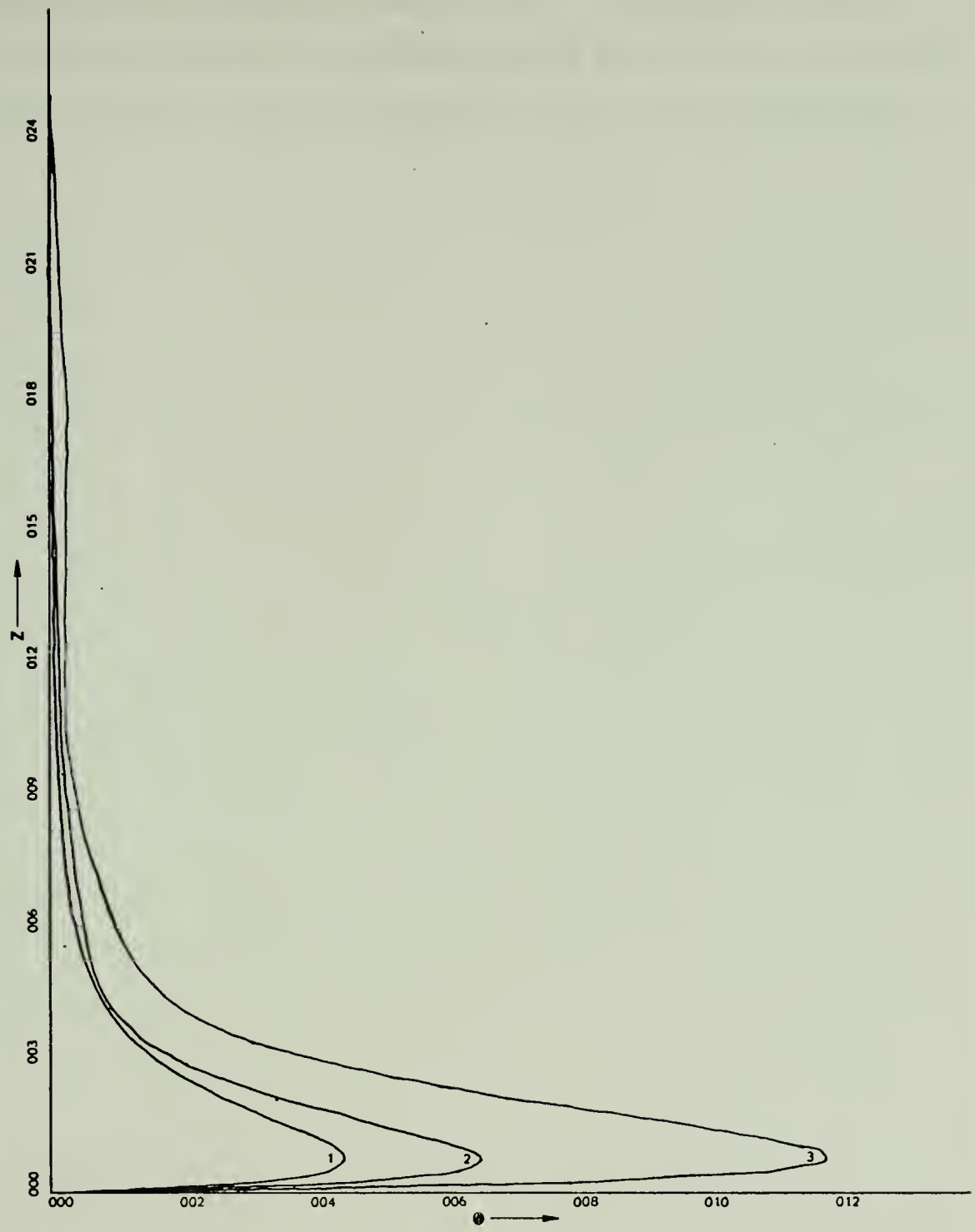

Figure 14. Distribution of disturbance potential temperature (θ in °K) with height (z in meters) utilizing series 9 for wave number (k) equal, respectively, to: 1) 0.275 m^{-1}; 2) 0.125 m^{-1}; 3) 0.050 m^{-1}.

exception of the point where U = c. The numerical solutions show that the presence of such points does not change the conclusion that the buoyancy term is that unimportant.

VI. CONCLUSIONS

In this study the numerical results of Stauffer (1973) were extended with the addition of buoyancy effects and two different lower boundary conditions. The buoyancy effects have no appreciable affect on the stream function and wind stress fields; however, the presence of buoyancy effects could affect the Reynolds wave stress through modifications in the mean wind profile. These effects were not considered in this study.

In this thesis, emphasis was placed on modifications in the mean profile which arose from the Reynolds wave stress. The two new boundary conditions which were investigated involved two methods of estimating $\frac{\partial U}{\partial z}$ in one of the lower boundary conditions. This term was entirely neglected in the study by Stauffer (1973). In the first method the derivative was evaluated from the logarithmic wind profile evaluated at a false level (z_1). This procedure leads to very large wave stresses near the surface when z_1 became small.

In the second method, $\frac{\partial U}{\partial z}$ was evaluated by finite differences. Many solutions were performed with this boundary condition involving different values of the wave number, convergence criteria, and the grid size. Those solutions showed that the wind profile was near the logarithmic profile for the larger wave numbers of order one.

Smaller wave numbers showed considerable fluctuation about the logarithmic profile in the lower layers with the tendency toward wind speeds larger than those given by the logarithmic profile. Figure 7, which employs the smallest grid size, shows this tendency clearly. However, further investigations with this profile suggest larger fluctuations if a finer convergence criteria is used. In general the computed wind profiles are consistent with observational data analyzed by Davidson (1974).

Further investigations of this type must carefully consider the lower boundary condition which was shown to be very sensitive in this study. Perhaps a full two-dimensional treatment of the air flow over the wave surface is required. Also it is very important to obtain accurate expressions for the turbulent exchange coefficients at different locations near the wave surfaces. These studies should be coordinated with careful analysis of observational data.

LIST OF REFERENCES

1. Davidson, K. L., 1974: "Observational Results on the Influence of Stability and Wind-wave Coupling on Momentum Transfer and Turbulent Fluctuations over Ocean Waves." Boundary-Layer Meteorology (in press), 5, 123-145.

2. Matsuno, T., 1966: "Numerical Integrations of the Primitive Equations by a Simulated Backward Difference Method." Journal of the Meteorological Society of Japan, 44, 1, 76-84.

3. Newman, R. L., 1969: A Theoretical Investigation of the Structure of Easterly Waves. M.S. Thesis, Naval Postgraduate School, Monterey, California, 67 pp.

4. _____ . Personal interview with R. Davis, Professor, Scripps Institute of Oceanography, LaJolla, California, April, 1973.

5. Richtmyer, R. D., 1957: Difference Methods for Initial Value Problems. Interscience Publishers, Inc., New York.

6. Stauffer, B. C., 1973: Application of a Theoretical Model to Velocity Fields Observed over Water Waves. M.S. Thesis, Naval Postgraduate School, Monterey, California, 66 pp.

7. Yefimov, V. V., 1970: "On the Structure of the Wind Velocity Field in the Atmospheric Near-water Layer and the Transfer of the Wind Energy to Sea Waves." Atmospheric and Oceanic Physics, 6, 10, 1043-1958, translated by McIntosh, J.D.L.

INITIAL DISTRIBUTION LIST

		No. Copies
1.	Defense Documentation Center Cameron Station Alexandria, Virginia 22314	2
2.	Library, Code 0212 Naval Postgraduate School Monterey, California 93940	2
3.	Naval Oceanographic Office Library (Code 3330) Washington, D. C. 20373	1
4.	Commander, Naval Weather Service Command Naval Weather Service Headquarters Washington Navy Yard Washington, D. C. 20390	1
5.	Dr. R. T. Williams, Code 51Wu Department of Meteorology Naval Postgraduate School Monterey, California 93940	10
6.	Lieutenant K. G. Dunning Naval Destroyer School Newport, Rhode Island 02840	3
7.	Lieutenant Commander B. C. Stauffer Fleet Numerical Weather Facility Naval Postgraduate School Monterey, California 93940	1
8.	Naval Weather Service Command Washington Navy Yard Washington, D. C. 20390	1
9.	Officer in Charge Environmental Prediction Research Facility Naval Postgraduate School Monterey, California 93940	1
10.	Commanding Officer U. S. Fleet Weather Central COMNAVMARIANAS, Box 12 FPO San Francisco, California 96630	1

11. Commanding Officer — 1
Fleet Weather Facility
P. O. Box 85
Naval Air Station
Jacksonville, Florida 32212

12. Commanding Officer — 1
U. S. Fleet Weather Facility
Box 72
FPO New York, New York 09510

13. Commanding Officer — 1
Fleet Numerical Weather Central
Naval Postgraduate School
Monterey, California 93940

14. Commanding Officer — 1
U. S. Fleet Weather Central
Box 110
FPO San Francisco, California 96610

15. Commanding Officer — 1
U. S. Fleet Weather Central
Box 31
FPO New York, New York 09540

16. Commanding Officer — 1
U. S. Fleet Weather Facility, Box 30
FPO San Francisco, California 96652

17. AFCRL - Research Library — 1
L. G. Hanscom Field
Attn: Nancy Davis/Stop 29
Bedford, Massachusetts 01730

18. Director, Naval Research Laboratory — 1
Attn: Tech. Services Information Officer
Washington, D. C. 20390

19. American Meteorological Society — 1
45 Beacon Street
Boston, Massachusetts 02128

20. Department of Meteorology — 3
Code 51
Naval Postgraduate School
Monterey, California 93940

21. Department of Oceanography — 1
Code 58
Naval Postgraduate School
Monterey, California 93940

22. Office of Naval Research — 1
Department of the Navy
Washington, D. C. 20360

23. Commander, Air Weather Service — 2
Military Airlift Command
United States Air Force
Scott Air Force Base, Illinois 62226

24. Atmospheric Sciences Library — 1
National Oceanic and Atmospheric
Administration
Silver Spring, Maryland 20910

25. Professor Victor Starr — 1
Department of Meteorology
Massachusetts Institute of Technology
Cambridge, Massachusetts 03139

26. Dr. J. Pedlosky — 1
Department of Geophysical Science
University of Chicago
Chicago, Illinois 60637

27. Dr. Joanne Simpson — 1
Experimental Meteorology Branch
National Oceanic and Atmospheric
Administration
Coral Gables, Florida 33124

28. National Center for Atmospheric Research — 1
Box 1470
Boulder, Colorado 80302

29. Dr. Fred Shuman, Director — 1
National Meteorological Center
National Oceanic and Atmospheric
Administration
Suitland, Maryland 20390

30. Dr. J. Smagorinsky, Director — 1
Geophysical Fluid Dynamics Laboratory
Princeton University
Princeton, New Jersey 08540

31. Professor N. A. Phillips — 1
Department of Meteorology
Massachusetts Institute of Technology
Cambridge, Massachusetts 02139

32. Dr. A. Schoenstadt — 1
Department of Mathematics, Code 53Zh
Naval Postgraduate School
Monterey, California 93940

33. Professor J. G. Charney — 1
54-1424
M.I.T.
Cambridge, Massachusetts 02139

34. Dr. M. G. Wurtele — 1
Department of Meteorology
UCLA
Los Angeles, California 90024

35. Dr. A. Arakawa — 1
Department of Meteorology
UCLA
Los Angeles, California 90024

36. Dr. G. Haltiner, Chairman — 1
Department of Meteorology
Naval Postgraduate School
Monterey, California 93940

37. Dr. R. L. Haney — 1
Department of Meteorology, Code 51Hy
Naval Postgraduate School
Monterey, California 93940

38. Dr. R. L. Elsberry — 1
Department of Meteorology, Code 51Es
Naval Postgraduate School
Monterey, California 93940

39. Dr. C.-P. Chang — 1
Department of Meteorology, Code 51Cj
Naval Postgraduate School
Monterey, California 93940

40. Dr. R. J. Renard — 1
Department of Meteorology, Code 51Rd
Naval Postgraduate School
Monterey, California 93940

41. Dr. K. L. Davidson — 5
Department of Meteorology, Code 51Ds
Naval Postgraduate School
Monterey, California 93940

42. Dr. S. Piacsek — 1
Code 7750
Naval Research Laboratory
Washington, D. C. 20390

43. Dr. D. Houston — 1
Department of Meteorology
University of Wisconsin
Madison, Wisconsin 53706

44. Dr. J. Holton 1
Department of Atmospheric Sciences
University of Washington
Seattle, Washington 98105

45. Dr. J. Young 1
Department of Meteorology
University of Wisconsin
Madison, Wisconsin 53706

46. Dr. R. Alexander 1
The Rand Corporation
1700 Main Street
Santa Monica, California 90406

47. Dr. W. L. Gates 1
The Rand Corporation
1700 Main Street
Santa Monica, California 90406

48. Dr. S. Rosenthal 1
National Hurricane Research Laboratory
P. O. Box 8265
University of Miami Beach
Coral Gables, Florida 33124

49. Mr. Tom Baxter 1
Environmental Prediction Research Facility
Naval Postgraduate School
Monterey, California 93940

50. Dr. R. E. Davis 1
University of California at San Diego
San Diego, California 92037

51. Dr. J. W. Miles 1
University of California at San Diego
San Diego, California 92037

52. Dr. O. M. Phillips 1
John Hopkins University
Baltimore, Maryland 21218

53. Dr. W. C. Reynolds 1
Department of Mechanical Engineering
Stanford University
Palo Alto, California 94305

54. Dr. D. J. Portman 1
Department of Meteorology
University of Michigan
Ann Arbor, Michigan 48105

55. Professor T. Green 1
Department of Meteorology
University of Wisconsin
Madison, Wisconsin 53706

SECURITY CLASSIFICATION OF THIS PAGE (When Data Entered)

REPORT DOCUMENTATION PAGE

READ INSTRUCTIONS BEFORE COMPLETING FORM

1. REPORT NUMBER	2. GOVT ACCESSION NO. / 3. RECIPIENT'S CATALOG NUMBER
4. TITLE (and Subtitle): Numerical Prediction of the Mean Wind Over Water Waves	5. TYPE OF REPORT & PERIOD COVERED: Master's Thesis, March 1974
	6. PERFORMING ORG. REPORT NUMBER
7. AUTHOR(s): Kenneth G. Dunning	8. CONTRACT OR GRANT NUMBER(s)
9. PERFORMING ORGANIZATION NAME AND ADDRESS: Naval Postgraduate School, Monterey, California 93940	10. PROGRAM ELEMENT, PROJECT, TASK AREA & WORK UNIT NUMBERS
11. CONTROLLING OFFICE NAME AND ADDRESS: Naval Postgraduate School, Monterey, California 93940	12. REPORT DATE: March 1974 / 13. NUMBER OF PAGES: 54
14. MONITORING AGENCY NAME & ADDRESS (if different from Controlling Office): Naval Postgraduate School, Monterey, California 93940	15. SECURITY CLASS. (of this report): Unclassified / 15a. DECLASSIFICATION/DOWNGRADING SCHEDULE

16. DISTRIBUTION STATEMENT (of this Report)

Approved for public release; distribution unlimited.

17. DISTRIBUTION STATEMENT (of the abstract entered in Block 20, if different from Report)

18. SUPPLEMENTARY NOTES

19. KEY WORDS (Continue on reverse side if necessary and identify by block number)

20. ABSTRACT (Continue on reverse side if necessary and identify by block number)

Stauffer (1973) developed a theoretical model for the prediction of the air flow above ocean waves. In this study his results were extended with the addition of buoyancy effects and two different lower boundary conditions.

Through numerical solutions it was possible to determine that: 1) mean wind velocities at lower levels closely approximate the initial mean velocity profile for large

DD FORM 1 JAN 73 1473 EDITION OF 1 NOV 65 IS OBSOLETE
S/N 0102-014-6601 | SECURITY CLASSIFICATION OF THIS PAGE (When Data Entered)
(Page 1)

wave numbers ($k \geq 0.45 m^{-1}$) or small wave amplitudes, 2) mean wind velocities at lower levels fluctuate more from the initial mean velocity profile as the wave number decreases or the wave amplitude increases, 3) solutions were very sensitive to the level where the velocity gradient is computed in the lower boundary condition, 4) disturbance potential temperature at lower levels increases inversely with wave number, and 5) the presence of temperature fluctuations has an insignificant effect on the Reynolds stress or on the stream function. The numerical solutions show general agreement with the observational analyses of wave modified wind profiles by Davidson (1974). However, these comparisons are not conclusive because of the sensitivity in the lower boundary condition.

Thesis
D793 Dunning
c.1 Numerical prediction
of the mean wind over
water waves.
149795